Journal of Zhejiang University-SCIENCE A (Applied Physics & Engineering)
ISSN 1673-565X (Print); ISSN 1862-1775 (Online)
www.zju.edu.cn/jzus; www.springerlink.com
E-mail: jzus@zju.edu.cn

# Residual stress analysis and bow simulation of crystalline silicon solar cells

Chih-Hung CHEN[1], Hsuan-Teh HU[†‡1], Fu-Ming LIN[2], Hsin-Hsin HSIEH[2]
([1]*Department of Civil Engineering, National Cheng Kung University, Tainan 701, China*)
([2]*Green Energy & Environment Research Laboratories, Industrial Technology Research Institute, Hsinchu 310, China*)
[†]E-mail: hthu@mail.ncku.edu.tw

Received Oct. 21, 2015; Revision accepted Apr. 7, 2016; Crosschecked Dec. 12, 2016

**Abstract:** The pressure to reduce solar energy costs encourages efforts to reduce the thickness of silicon wafers. Thus, the cell bowing problem associated with the use of thin wafers has become increasingly important, as it can lead to the cracking of cells and thus to high yield losses. In this paper, a systematic approach for simulating the cell bowing induced by the firing process is presented. This approach consists of three processes: (1) the material properties are determined using a nanoidentation test; (2) the thicknesses of aluminum (Al) paste and silver (Ag) busbars and fingers are measured using scanning electron microscopy; (3) non-linear finite element analysis (FEA) is used for simulating the cell bowing induced by the firing process. As a result, the bowing obtained using FEA simulation agrees better with the experimental data than that using the bowing calculations suggested in literature. In addition, the total in-plane residual stress state in the wafer/cell due to the firing process can be determined using the FEA simulation. A detailed analysis of the firing-induced stress state in single crystalline silicon (sc-Si), cast, and edge-defined film-fed growth (EFG) multi-crystalline silicon wafers of different thicknesses is presented. Based on this analysis, a simple residual stress calculation is developed to estimate the maximum in-plane principal stress in the wafers. It is also proposed that the metallization pattern, Ag busbars and fingers screen printed on the front of a solar cell, can be designed using this approach. A practical case of a 3-busbar Si solar cell is presented.

**Key words:** Bow; Solar cell; Silicon solar cell; Finite element analysis (FEA); Residual stress
http://dx.doi.org/10.1631/jzus.A1500279 **CLC number:** TB12; TB30

## 1 Introduction

The most critical processing step during the manufacture of screen-printed (SP) solar cells is the firing process. In order to maintain low series resistance, aluminum (Al) paste and silver (Ag) busbars and fingers are used to form SP contacts for most industrial solar cells. Cell bowing and residual stress are formed due to a mismatch of the thermal coefficient of expansion (TCE) and the different mechanical behavior of the materials involved between SP contacts and a silicon (Si) wafer. The wafer bows and forms a convex or concave body upon cooling. As increasingly larger and thinner Si wafers are manufactured to reduce the cost per watt of photovoltaic power, cell bowing and residual stress become serious problems for modulus assembly and reliability.

A bowing is defined as the measured deflection at the center of the wafer from the mid-point of the substrate to the plane connecting the wafer edges, and it should be 1 mm or less for module assembly (Hilali *et al.*, 2007). The bowing of solar cells has been extensively studied, with techniques developed to reduce it (Schneider *et al.*, 2001; Bähr *et al.*, 2005; Huster, 2005a; 2005b; Möller *et al.*, 2005; Bittoni *et al.*, 2006; Hilali *et al.*, 2007). Cell bowing can be

---

[‡] Corresponding author

ORCID: Hsuan-Teh HU, http://orcid.org/0000-0001-8582-0670

modeled as a bimetallic strip, bending in only one dimension:

$$\delta=\frac{3(\alpha_{\mathrm{Al}}-\alpha_{\mathrm{Si}})(T_{\mathrm{f}}-T_{\mathrm{m}})(t_{\mathrm{Al}}+t_{\mathrm{Si}})L^2}{4t_{\mathrm{Al}}^2\left[4+6\frac{t_{\mathrm{Si}}}{t_{\mathrm{Al}}}+4\left(\frac{t_{\mathrm{Si}}}{t_{\mathrm{Al}}}\right)^2+\left(\frac{E_{\mathrm{Si}}}{E_{\mathrm{Al}}}\right)\left(\frac{t_{\mathrm{Si}}}{t_{\mathrm{Al}}}\right)^3+\left(\frac{E_{\mathrm{Al}}}{E_{\mathrm{Si}}}\right)\frac{t_{\mathrm{Al}}}{t_{\mathrm{Si}}}\right]},\quad(1)$$

where $\alpha_{\mathrm{Si}}$ is the TCE of the Si wafer, $\alpha_{\mathrm{Al}}$ is the TCE of the Al paste, $t_{\mathrm{Si}}$ is the thickness of the Si wafer, $t_{\mathrm{Al}}$ is the thickness of the Al paste, $E_{\mathrm{Si}}$ is the elastic modulus of the Si wafer, $E_{\mathrm{Al}}$ is the elastic modulus of the Al paste, $T_{\mathrm{f}}$ is the solidification temperature of the Al paste, $T_{\mathrm{m}}$ is the room temperature, and $L$ is the length of the solar cell. However, the results of Eq. (1) do not agree well with experiment results. In order to match experimental results, plastic deformation was considered by Huster (2005a), who modified Eq. (1) by neglecting insignificant terms:

$$\delta=\frac{3L^2}{4}\frac{t_{\mathrm{Al}}}{t_{\mathrm{Si}}^2}\frac{\sigma_{\mathrm{Al,yielding}}}{E_{\mathrm{Si}}},\quad(2)$$

where $\sigma_{\mathrm{Al,yielding}}$ is the yielding stress of the Al paste. The bowing obtained using Eq. (2) is more accurate than that obtained using Eq. (1), but the yielding stress of Al paste is difficult to obtain through experiment. Hilali *et al.* (2007) modified the calculation of cell bowing by considering the real coverage area of the Al paste on the Si wafer:

$$\delta=\frac{A_{\mathrm{f}}\times3(\alpha_{\mathrm{Al}}-\alpha_{\mathrm{Si}})(T_{\mathrm{f}}-T_{\mathrm{m}})(t_{\mathrm{Al}}+t_{\mathrm{Si}})L^2}{4t_{\mathrm{Al}}^2\left[4+6\frac{t_{\mathrm{Si}}}{t_{\mathrm{Al}}}+4\left(\frac{t_{\mathrm{Si}}}{t_{\mathrm{Al}}}\right)^2+\left(\frac{E_{\mathrm{Si}}}{E_{\mathrm{Al}}}\right)\left(\frac{t_{\mathrm{Si}}}{t_{\mathrm{Al}}}\right)^3+\left(\frac{E_{\mathrm{Al}}}{E_{\mathrm{Si}}}\right)\frac{t_{\mathrm{Al}}}{t_{\mathrm{Si}}}\right]},\quad(3)$$

where $A_{\mathrm{f}}$ is the area coverage factor. However, this parameter is also difficult to obtain experimentally, and Eq. (3) is proposed for back-contact silicon solar cells. The influence of the Ag busbars and fingers on cell bowing was neglected in these studies. In order to better understand the influence of Ag busbars and fingers on cell bowing, Brown *et al.* (2009) used the finite element method (FEM) to analyze the cell bowing induced by the firing process. However, the calculated bowing was not consistent with experiment. Similarly, Yu *et al.* (2012) simulated cell bowing with a boron back surface field based on the FEM, but did not compare the results with experimental results. Although the bowing calculated using the FEM was no more accurate than that obtained using the modified bimetallic strip model, other important information such as stress, strain, or plastic deformation can be obtained using the FEM rather than the modified bimetallic strip model.

In respect to the residual stresses, the in-plane residual stresses on Czochralski (Cz), cast, and edge-defined film-fed growth (EFG) multi-crystalline silicon (mc-Si) wafers have been measured using infrared polariscopy, photoluminescence, photoelasticity, non-linear resonance ultrasonic vibrations, and X-ray topography (Yasutake *et al.*, 1982; He *et al.*, 2004; Brito *et al.*, 2005a; 2005b; Best *et al.*, 2006; He and Danyluk, 2006; Li *et al.*, 2006). However, these measurements provide only the average through-thickness residual in-plane shear stress, not the complete residual stress state in the wafer. These investigations focused on the residual stresses induced by crystal growth or slicing in the Si wafer. After the solar cell process, these measurements become invalid because the Si wafer is covered by the Ag busbars and fingers. When direct measurements cannot be performed on the solar cells after the solar cell process, FEM can provide the complete residual stress state.

A FEM simulation of cell bowing induced by the firing process can help researchers to better understand the cell bowing problem and will provide the complete in-plane residual stress state for further investigation. This paper proposes a systematic approach that uses the material properties obtained using a nanoindentation test, the thicknesses of the Si wafer, Ag busbars and fingers, and Al paste measured using scanning electron microscopy (SEM), and non-linear finite element analysis (FEA) to calculate the cell bowing and the complete residual stress state. The FEA results are compared with bowing calculations obtained using Eqs. (2) and (3).

## 2 Experimental procedure

The standard industrial solar cell process was adopted to manufacture single crystalline silicon (sc-Si) solar cells. Si wafers were etched using the chemical method to control the thickness at 110, 120, 150, 170, and 200 μm, respectively. At least three solar cells were manufactured for each Si wafer thickness. After phosphorous diffusion, the wafers were doped on one surface, making it n-type Si, with the remaining wafer being p-type Si. An antireflective (AR) coating layer was deposited on the n-type Si. The SP contacts, Al paste on the rear side and Ag busbars and fingers on the front side, were screen-printed using Ag and Al metallic inks and co-fired in an infrared belt drive furnace. The firing conditions were fixed. The temperature profile for the belt furnace is shown in Fig. 1. After firing, the bowing of the solar cells was measured using an optical method with the quick vision system (Mitutoyo, Japan).

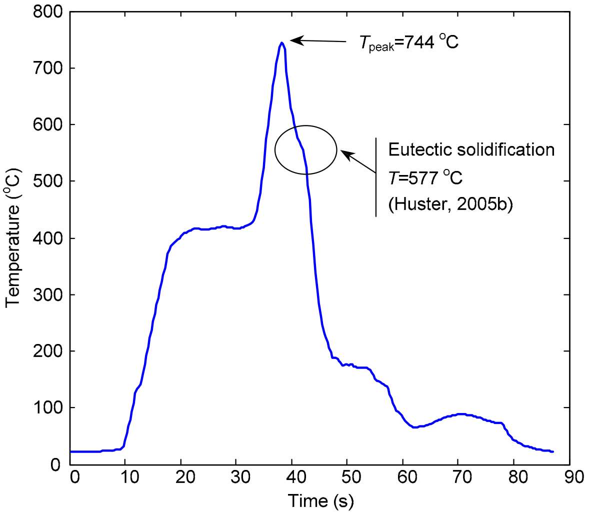

**Fig. 1 Temperature profile of firing process**

The nanoindentation method was used to determine the elastic modulus and hardness of the Ag busbars and Al paste. The force-displacement curves generated during the loading and unloading steps were converted following ISO 14577 (ISO, 2015), as shown in Fig. 2. The complex structure of a solar cell does not satisfy the flatness requirement for the nanoidentation test. The substrate (Si wafer) leads to inaccurate elastic properties of the Al paste and Ag busbars and fingers calculated from the loading step of the nanoidentation test (Saha and Nix, 2002). In order to avoid the influence of the substrate, Young's modulus was calculated from the unloading step in the nanoidentation test. When the indentation depth is less than the thickness of the thin film, the influence of the substrate can be neglected.

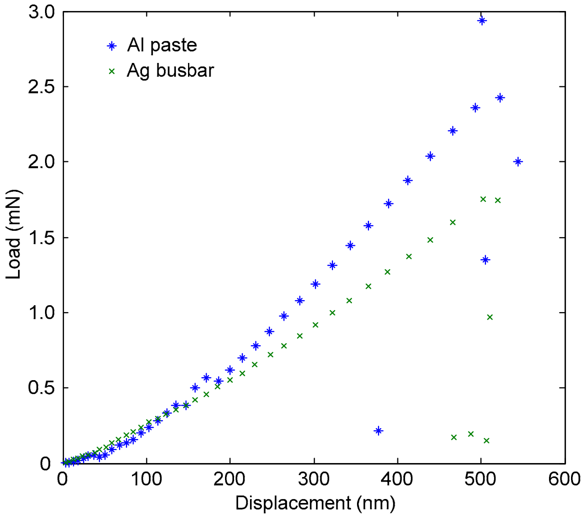

**Fig. 2 Load vs. indentation depth for Al paste and Ag busbar**

The thicknesses of the Si wafer and Ag busbars and fingers were measured by SEM. The SEM cross-sectional image of the solar cell is shown in Fig. 3. Because the firing conditions were fixed, the influence of the Si wafer thickness was neglected. The thickness of the Ag busbars and fingers was thus the same for different thicknesses of the Si wafer in the FEA simulation.

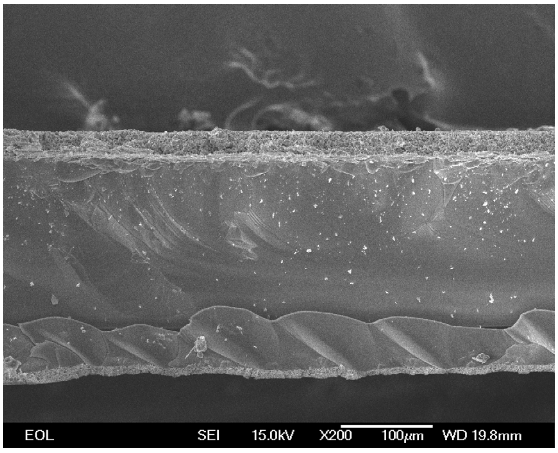

**Fig. 3 SEM cross-sectional micrograph of conventional Si solar cell**

## 3 Finite element analysis model

The geometric parameters and material properties of the sc-Si solar cell were obtained from experiments to simulate cell bowing after the firing process. According to the profile of the firing temperature, a liquid phase formed between the Al paste and the Si wafer and no stress was induced. When the temperature dropped below the Al-Si eutectic temperature of 577 °C (Fig. 1), all materials of the solar cell began to solidify and contract. Therefore, an initial temperature of 577 °C was applied in the FEA model to analyze the bowing and residual stresses induced by cooling down to room temperature (25 °C). The FEA model was built and solved by standard FEA software ABAQUS®. Various Si wafer types, such as EFG and cast mc-Si wafers, for solar cells with different geometric parameters and material properties were simulated.

### 3.1 Model geometry

The geometric parameters of solar cells with different Si wafers are shown in Fig. 4 and listed in Table 1, where $L_c$ is the length of the solar cell, $L_a$ is the length of Al paste, $B$ is the half distance between two Ag busbars, $S$ is the distance between Ag fingers, $W_b$ is the width of an Ag busbar, $t_w$ is the thickness of the Si wafer, $t_a$ is the thickness of Al paste, and $t_b$ is the thickness of Ag busbars. The size of the sc-Si solar cells was 125 mm×125 mm and the corners were curved, not rectangular, as shown by the dashed line in Fig. 4. The sizes of the cast mc-Si solar cell were 125 mm×125 mm and 156 mm×156 mm, and the size of the EFG solar cell was 100 mm×100 mm. The corners of the cast and EFG mc-Si wafer simulated by FEA were rectangular as shown by the solid line in Fig. 4. The distances between each Ag finger and the width of the Ag busbar were fixed in the FEA model. The thickness of the Al paste was 30 μm and that of an Ag busbar was 10 μm, as measured by SEM.

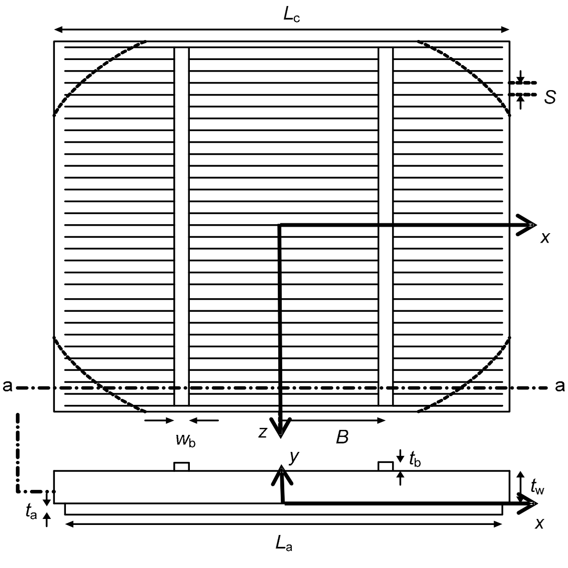

**Fig. 4 Schematic view of Si solar cell showing the geometric parameters**

**Table 1 Geometric parameters of solar cells (unit: mm)**

| Wafer type | $L_w$ | $L_a$ | $S$ | $W_b$ | $B$ |
|---|---|---|---|---|---|
| sc-Si wafer | 125 | 122 | 2.1 | 2 | 29.5 |
| Cast wafer | 125 | 122 | 2.1 | 2 | 29.5 |
| Cast wafer | 156 | 153 | 2.1 | 2 | 37.0 |
| EFG wafer | 100 | 97 | 2.1 | 2 | 23.0 |

### 3.2 Material properties

An sc-Si wafer is anisotropic. The fourth-order elastic stiffness matrix was used (Funke *et al.*, 2004):

$$\boldsymbol{C}_{ijkl}=\begin{bmatrix}165.64 & 63.94 & 63.94 & 0 & 0 & 0\\ & 165.64 & 63.94 & 0 & 0 & 0\\ & & 165.64 & 0 & 0 & 0\\ & & & 79.51 & 0 & 0\\ & \text{sym.} & & & 79.51 & 0\\ & & & & & 79.51\end{bmatrix}\text{GPa}. \tag{4}$$

The cast mc-Si wafer was assumed to be elastic and isotropic. The Young's modulus and Poisson's ratio for cast silicon ($E$=162.5 GPa, $v$=0.223) reported by Funke *et al.* (2004) were used.

Although EFG wafers are multi-crystalline in nature, they are known to have a predominant grain orientation due to the growth process. Specifically, EFG wafers are characterized by a {1 1 0} surface and a <1 1 2> growth direction. Therefore, the stiffness is specified using the {1 1 0} single-crystal properties with the $[1\,\bar{1}\,2]$, $[\bar{1}\,1\,1]$, and [1 1 0] orientations representing the $x$-, $y$-, and $z$-axes, respectively. The resulting elastic stiffness matrix for the EFG wafer is given by (Brun and Melkote, 2009)

$$\boldsymbol{C}_{ijkl}^{\mathrm{EFG}}=\begin{bmatrix} 203.85 & 44.83 & 44.83 & 0 & 0 & 0 \\ & 194.30 & 54.38 & -13.51 & 0 & 0 \\ & & 194.30 & 13.51 & 0 & 0 \\ & & & 60.40 & 0 & 0 \\ & \text{sym.} & & & 60.40 & 13.51 \\ & & & & & 69.96 \end{bmatrix}\text{GPa}. \tag{5}$$

The linear TCE of a Si wafer is $3.5\times10^{-6}$ $\mathrm{K}^{-1}$ (Huster, 2005a). It was assumed that all Si wafer types had the same TCE. The TCE of Al paste and Ag fingers are listed in Table 2. The perfect elasticity plastic model was used to simulate the material behavior of the Al paste and Ag busbars and fingers. Plastic flow occurred when the stress reached the yielding stress and there was no stress increase when the plastic strain increased. The Young's modulus, Poisson's ratio, and yielding stress ($\sigma_\mathrm{y}$) of the Al paste and Ag busbars and fingers measured from the nanoindentation test are listed in Table 2.

**Table 2 Material properties of Al and Ag**

| Material | $E$ (GPa) | $v$ | $\sigma_\mathrm{y}$ (MPa) | TCE ($\times10^{-6}$ $\mathrm{K}^{-1}$) |
|---|---|---|---|---|
| Al | 25.5 | 0.35 | 15 | 23.1 |
| Ag | 32.7 | 0.33 | 69 | 16.5 |

### 3.3 Boundary conditions

In order to reduce computation time, a quarter of a solar cell was modeled for FEA because of the symmetry along the busbar and finger directions. The directions along the finger and busbar were defined as the $x$- and $z$-coordinates, respectively, and the thickness direction was defined as the $y$-direction as shown in Fig. 4. The center of the solar cell was defined as the coordinate origin. The symmetric boundary conditions along the $x$-direction ($u_x=\theta_{xy}=\theta_{xz}=0$) were set in the $yz$ plane ($x=0$) and those along the $z$-direction ($u_z=\theta_{yz}=\theta_{xz}=0$) were set in the $xy$ plane ($z=0$). In order to avoid rigid body motion along the thickness direction in the FEA model, we set the displacement along the thickness direction to be zero ($u_y=0$) in a corner of the solar cell.

### 3.4 Mesh grid independence

The quality of FEA simulation is related to the mesh grid density. A denser mesh grid results in more reliable FEA simulations at the cost of higher computation time. The element aspect ratio, defined as the ratio of the longest edge to the shortest edge of an element, should not be greater than 4 in a 3D FEA model. For a solar cell, the thickness dimension is much less than the other dimensions. The 3D element size that is small enough to satisfy the aspect ratio requirement causes too dense mesh and too much computation time. Therefore, 3D solid elements were not used in this paper. The FEA model of the solar cell used SC8R elements for the Si wafer, Al paste, and Ag busbars and T3D2 elements for the Ag fingers. The interfaces between the Ag busbars and the Si wafer, and the Si wafer and the Al paste were assumed to be perfectly bonded. The nodes of interfaces have the same displacement in the different materials. According to convergence analysis, the mesh corresponding to a 2-mm seed size was considered to be adequate for all wafer types. Although non-linear material behavior was being considered, the simulation times for all models were reasonable (less than 1 h).

## 4 Results and discussion

FEA simulation results of the sc-Si solar cell after the firing process are shown in Fig. 5. The bowing is obtained by measuring the maximum displacement from the plane containing the bottom of the corner edges to the top edge of the side of the solar cell at the centerline planes. The deformed shape in the FEA simulation is similar to the real deformed shape of a solar cell induced by the firing process. The FEA simulation results and bowing calculations are compared with experimental results for various Si wafer thickness in Fig. 6. The FEA results are in better agreement with the experimental data than those of the bowing calculations. One explanation for this is that the bowing calculations are based on a 1D bimetallic strip model. They assume that the Si wafer is isotropic and elastic, but the sc-Si wafer is actually anisotropic. In addition, only the Si wafer and the Al paste are considered in the bowing calculations.

The contributions of the Ag busbars and fingers to cell bowing are neglected, which may lead to inaccurate results. The 1D assumption of a bimetallic strip may cause inaccuracy. Comparing with the bowing calculations, we can observe that the results of Eq. (2) are closer to the experimental results than those of Eq. (3). In addition, the calculation of Eq. (2) is more simple and convenient.

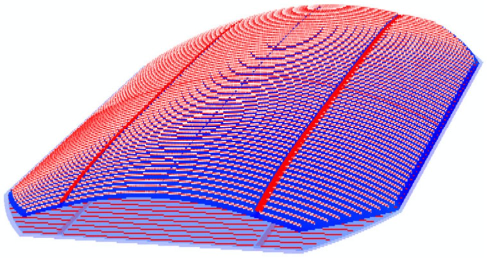

**Fig. 5 FEA simulation results of cell bowing induced by firing process**

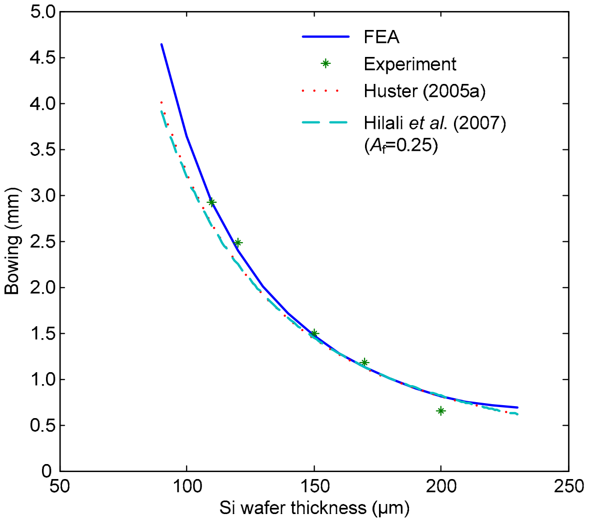

**Fig. 6 FEA results and other bowing calculations compared with experimental results**

The FEA simulation provides more accurate bowing calculations and other information, such as residual stress, for better understanding cell bowing and can thus be used in investigations such as breakage and reliability analysis. As mentioned earlier, FEA simulation takes anisotropic materials into consideration and allows Si wafers manufactured using different growth processes to be compared, which is not possible using Eqs. (2) and (3). Fig. 7 shows the maximum in-plane principal tensile stress distribution on different Si wafer surfaces induced by the firing process for a wafer thickness of 200 μm. The higher residual stresses along the busbar and the lower residual stresses at the center of the Si wafer are

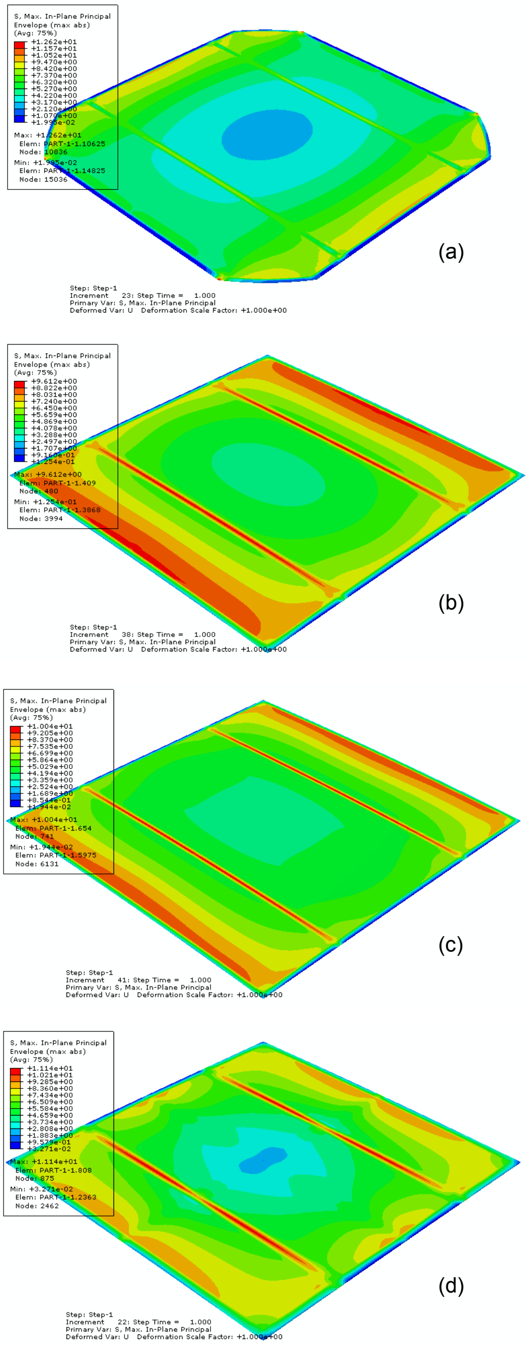

**Fig. 7 Typical maximum in-plane principal stress distributions**

(a) sc-Si wafer, 125 mm×125 mm; (b) Cast wafer, 125 mm×125 mm; (c) Cast wafer, 156 mm×156 mm; (d) EFG wafer, 100 mm×100 mm observed for all types of Si wafer. Residual stress distribution is related to the material properties of the Si wafer. The residual stress distributions on cast mc-Si wafer, with different wafer sizes, are similar (Figs. 7b and 7c). The residual stress distributions on the sc-Si and EFG wafers, which are anisotropic, are different from those on the cast wafer.

Fig. 8 shows the modeled data of bowing versus Si wafer thickness for different types of Si wafer. As expected, irrespective of wafer type, a decrease in Si wafer thickness leads to an increase in the bowing induced by the firing process. The cell bowing is mainly dominated by wafer size. The same wafer size of sc-Si and cast wafers, 125 mm×125 mm, results in a similar cell bowing. The largest wafer size of cast wafer, 156 mm×156 mm, shows the largest bowing, and the smallest wafer size of EFG wafer, 100 mm ×100 mm, the smallest bowing. The material properties of sc-Si, cast mc-Si, and EFG Si wafer are not the dominant factor for cell bowing.

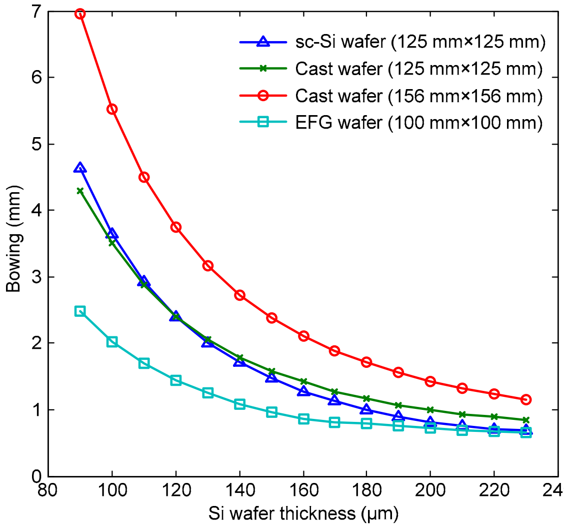

**Fig. 8 Bowing obtained using FEA simulation as a function of Si wafer thickness for various types of Si wafer**

The maximum in-plane principal tensile stresses, $\sigma_{\max}$, of the different types of Si wafer obtained from FEA simulation versus wafer thickness are plotted in Fig. 9. The maximum in-plane principal tensile stress increases with decreasing wafer thickness for all types of Si wafer. In contrast to cell bowing, the wafer size did not affect the magnitude of the maximum in-plane principal tensile stress. Hence, $\sigma_{\max}$ for the cast wafer with the different wafer sizes, 125 mm ×125 mm and 156 mm×156 mm, are very close. The results are consistent with the residual stress measurements performed by Brito *et al.* (2005a; 2005b) because the maximum residual stress is determined by the local force equilibrium between the Si wafer and the SP contacts. Therefore, the wafer size is not a dominant factor in the maximum residual stress. However, a larger wafer size does lead to greater cell bowing and thus a larger bending stress may be induced during handling, transport, assembly or other manufacturing processes. As the result, breakage of solar cells may easily occur during those processes and increase the costs of solar energy.

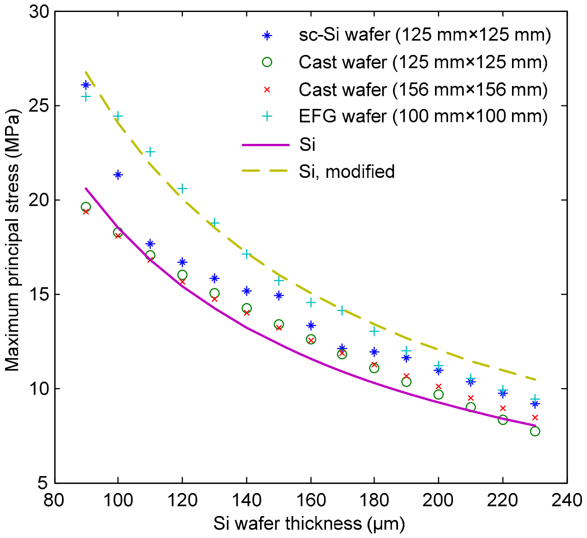

**Fig. 9 Maximum in-plane residual stress as a function of Si wafer thickness for various types of Si wafer obtained using FEA simulation and the residual stress equation**

The residual stress of the Al paste, and Ag busbars and fingers induced by the firing process was also obtained using FEA simulation. All residual stress states of SP contacts were tensile stresses and reached the yielding stress, in contrast, those of the Si wafer were compression stresses. Considering the local force equilibrium, the total compression force must be equal to the total tensile force, and thus we can easily calculate the residual stress of the Si wafer by

$$\sigma_{\mathrm{Si}}=\frac{t_{\mathrm{a}}}{t_{\mathrm{w}}}\sigma_{\mathrm{Al,yielding}}+\frac{t_{\mathrm{b}}}{t_{\mathrm{w}}}\sigma_{\mathrm{Ag,yielding}}, \tag{6}$$

where $\sigma_{\mathrm{Si}}$ is the maximum in-plane residual stress on the Si wafer, and $\sigma_{\mathrm{Ag,yielding}}$ is the yielding stress of the Ag busbar. The residual stresses calculated using Eq. (6) for various Si wafer thicknesses are plotted in Fig. 9 (solid line). The residual stresses of Si wafer calculated using Eq. (6) agree well with FEA results for cast mc-Si wafer, and the residual stress calculation using Eq. (6) is simpler than an FEA simulation. It can save much computation time. However, the sc-Si and EFG wafers are anisotropic and the residual stresses calculated using Eq. (6) are underestimated. A modification factor ($M_{\mathrm{f}}$) is suggested to be added to Eq. (6) for the sc-Si and EFG wafers (Eq. (7)). The $M_{\mathrm{f}}$ value for the sc-Si wafer and EFG wafers in this paper is 1.3.

$$\sigma_{\mathrm{Si}}=\left(\frac{t_{\mathrm{a}}}{t_{\mathrm{w}}}\sigma_{\mathrm{Al,yielding}}+\frac{t_{\mathrm{b}}}{t_{\mathrm{w}}}\sigma_{\mathrm{Ag,yielding}}\right)\times M_{\mathrm{f}}. \tag{7}$$

The residual stresses calculated using Eq. (7) for various Si wafer thicknesses are plotted in Fig. 9 (dashed line). For the EFG wafer, the residual stress calculated using Eq. (7) agrees better with the FEA results. However, the residual stress is overestimated for the sc-Si wafer. The stress concentration may occur due to geometrical discontinuity of the sc-Si wafer at the non-rectangular corner.

Breakage of a solar cell sometimes occurs not in the silicon wafer but in the Ag busbars or fingers and no information on the Ag busbars and fingers was obtained in previous studies. In this paper, the Ag busbar and fingers were assumed elasticly-perfect plastic to reduce the computation time. This assumption limited us to determining the location with a high possibility of breakage in the Ag busbar and fingers using residual stresses which were reaching the same yielding stress. However, the plastic strain can be used for this purpose. The authors helped a solar cell company to design a 3-busbar solar cell, as shown in Fig 10.

The breakage of the solar cells occurs not in the Si wafer but in the Ag busbar. FEA simulation provides the plastic strain distribution in the Ag busbar, as shown in Fig. 11. The position with the maximum plastic strain in the FEA simulation is consistent with the position of breakage in practice.

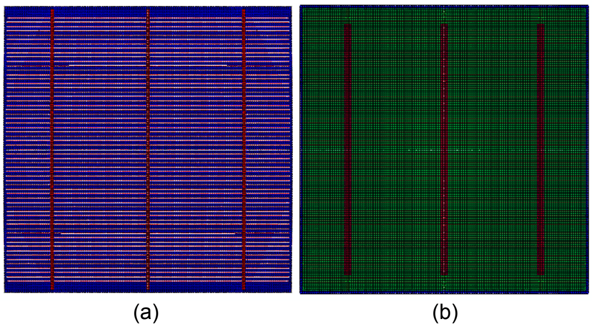

Fig. 10 Geometric shape of 3-busbar solar cell: front (a) and back (b) sides of the solar cell

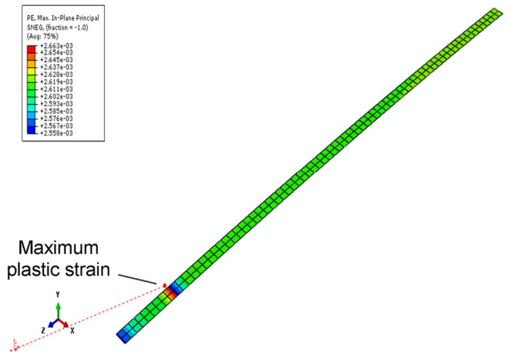

Fig. 11 Plastic strain distribution on busbar of 3-busbar solar cell

## 5 Conclusions

In conclusion, a systematic approach that uses the material properties obtained using a nanoindentation test, the thicknesses of the SP contacts measured using SEM, and the cell bowing simulated by FEA software was presented. It provides accurate bowing results that agree well with experiments and the complete in-plane principal stress distribution for various types of Si wafer. The maximum residual stress induced by the firing process of an Si wafer can be obtained using FEA simulation or Eq. (6) for a cast wafer or Eq. (7) for EFG and sc-Si wafers. Using Eqs. (6) and (7) to calculate residual stress is simple and can save much computation time. Because Ag busbars and fingers are considered in the FEA model, the metallized pattern for solar cells can be analyzed using FEA simulation. In this paper, plastic strain is proposed to estimate the possibility of breakage in the Ag busbar and finger.

## References

Bähr, M., Dauwe, S., Lawerenz, A., *et al.*, 2005. Comparison of bow-avoiding Al pastes for thin, large-area crystalline silicon solar cells. 20th European Photovoltaic Solar Energy Conference and Exhibition, p.926-929.

Best, S.R., Hess, D.P., Belyaev, A., *et al.*, 2006. Audible vibration diagnostics of thermo-elastic residual stress in multi-crystalline silicon wafers. *Applied Acoustics*, **67**(6): 541-549.
http://dx.doi.org/10.1016/j.apacoust.2005.09.004

Bittoni, L., Calvelli, R., Butturi, M.A., *et al.*, 2006. Aluminium pastes suitable for wide range thin crystalline silicon solar cells processing. Blistering and bowing effects reduction. 21st European Photovoltaic Solar Energy Conference and Exhibition, p.818-821.

Brito, M.C., Maia Alves, J., Serra, J.M., *et al.*, 2005a. Measurement of residual stress in EFG ribbons using a phase-shifting IR photoelastic method. *Solar Energy Materials and Solar Cells*, **87**(1-4):311-316.
http://dx.doi.org/10.1016/j.solmat.2004.07.028

Brito, M.C., Pereira, J.P., Maia Alves, J., *et al.*, 2005b. Measurement of residual stress in multicrystalline silicon ribbons by a self-calibrating infrared photoelastic method. *Review of Scientific Instruments*, **76**(1):013901.
http://dx.doi.org/10.1063/1.1823654

Brown, G.R., Levine, R.A., Shaikh, A., *et al.*, 2009. Three-dimensional solar cell finite-element sintering simulation. *Journal of the American Ceramic Society*, **92**(7):1450-1455.
http://dx.doi.org/10.1111/j.1551-2916.2009.03120.x

Brun, X.F., Melkote, S.N., 2009. Analysis of stresses and breakage of crystalline silicon wafers during handling and transport. *Solar Energy Materials and Solar Cells*, **93**(8): 1238-1247.
http://dx.doi.org/10.1016/j.solmat.2009.01.016

Funke, C., Kullig, E., Kuna, M., *et al.*, 2004. Biaxial fracture test of silicon wafers. *Advanced Engineering Materials*, **6**(7):594-598.
http://dx.doi.org/10.1002/adem.200400406

He, S., Danyluk, S., 2006. Residual stresses in polycrystalline silicon sheet and their relation to electron-hole lifetime. *Applied Physics Letters*, **89**(11):111909.
http://dx.doi.org/10.1063/1.2354308

He, S., Zheng, T., Danyluk, S., 2004. Analysis and determination of the stress-optic coefficients of thin single crystal silicon samples. *Journal of Applied Physics*, **96**(6):3103-3109.
http://dx.doi.org/10.1063/1.1774259

Hilali, M.M., Gee, J.M., Hacke, P., 2007. Bow in screen-printed back-contact industrial silicon solar cells. *Solar Energy Materials and Solar Cells*, **91**(13):1228-1233.
http://dx.doi.org/10.1016/j.solmat.2007.04.010

Huster, F., 2005a. Aluminium-back surface field: bow investigation and elimination. 20th European Photovoltaic Solar Energy Conference and Exhibition, p.635-638.

Huster, F., 2005b. Investigation of the alloying process of screen printed aluminium pastes for the BSF formation on silicon solar cells. 20th European Photovoltaic Solar Energy Conference and Exhibition, p.1466-1469.

ISO (International Organization for Standardization), 2015. Metallic Materials–Instrumented Indentaion Test for Hardness and Materials Parameters, ISO 14577-1:2015. ISO, Geneva.

Li, F., Garcia, V., Danyluk, S., 2006. Full field stress measurements in thin silicon sheet. Proceedings of the Fourth World Conference on Photovoltaic Energy Conversion, **1**:363-368.
http://dx.doi.org/10.1109/WCPEC.2006.279425

Möller, H.J., Funke, C., Rinio, M., *et al.*, 2005. Multicrystalline silicon for solar cells. *Thin Solid Films*, **487**(1-2): 179-187.
http://dx.doi.org/10.1016/j.tsf.2005.01.061

Saha, R., Nix, W.D., 2002. Effects of the substrate on the determination of thin film mechanical properties by nanoindentation. *Acta Materialia*, **50**(1):23-38.
http://dx.doi.org/10.1016/S1359-6454(01)00328-7

Schneider, A., Gerhards, C., Huster, F., *et al.*, 2001. Al BSF for thin screen-printed multi-crystalline Si solar cells. 17th European Photovoltaic Solar Energy Conference and Exhibition, p.1768-1771.

Yasutake, K., Uemno, M., Kawabe, H., *et al.*, 1982. Measurement of residual stress in bent silicon wafers by means of photoluminescence. *Japanese Journal of Applied Physics*, **21**(12):1715-1719.
http://dx.doi.org/10.1143/JJAP.21.1715

Yu, L., Jiang, Y., Lu, S., *et al.*, 2012. 3D FEM for sintering of solar cell with boron back surface field based on Solidwork Simulation. International Conference on Mechanical, Industrial, and Manufacturing Engineering, p.81-86.

## 中文概要

**题　目：**矽晶太阳能电池的翘曲模拟与残留应力分析

**目　的：**建立一套系统的方法来模拟矽晶太阳能电池的翘曲行为，进而分析因翘曲而产生的残留应力。

**创新点：**1. 利用纳米压痕实验及电子显微镜测量材料性质及结构尺寸，帮助有限元分析更准确地模拟太阳能电池的翘曲行为；2. 提出了 2 个针对不同矽晶太阳能电池因翘曲产生的简易残留应力的计算公式。

**方　法：**1. 利用纳米压痕实验测量铝胶及银胶的材料性质，使用电子显微镜测量铝胶及银胶的结构尺

寸；2. 建立非线性有限元分析模型并与实验结果进行比较（图 6），得出不同矽晶太阳能电池残留应力分布结果（图 7）；3. 将简易残留应力公式（公式（6）和（7））和有限元分析得到的结果进行比较（图 9）。

**结　论：** 1. 建立了一套有效模拟矽晶太阳能电池翘曲行为的分析方法，该方法包含 3 个部分:（1）纳米压痕实验测量铝胶和银胶的材料性质；（2）电子显微镜测量细部结构尺寸；（3）非线性有限元分析。利用此方法模拟的翘曲行为较其它计算方法更贴近实验结果。2. 该方法不仅能分析不同矽晶太阳能电池的翘曲行为，而且能提供除了翘曲以外的其它信息，比如残留应力。本文提出了 2 个较为简易的残留应力计算公式，计算不同矽晶太阳能电池因翘曲而产生的残留应力。3. 该方法考虑了银胶对矽晶太阳能电池翘曲的影响，在实际应用中可以帮助分析不同银胶的网印方式对矽晶太阳能电池翘曲的影响。本文以帮助某公司设计太阳能电池为例，证明了利用该分析方法在实际应用中帮助公司分析银胶网印的可行性。

**关键词：** 翘曲；矽晶太阳能电池；残留应力；有限元分析